One-Pot strategic synthesis of 1,3,5-pyrazoline derivatives using NiFe₂O₄.Cu(OH)₂ magnetic nanocomposite as heterogeneous catalyst and their theoretical studies as antifungal agents

Anjaneyulu Bendi[1] ⓘ, Priyanka Yadav[2] ⓘ, Aditi Tiwari[3] ⓘ, Anirudh Singh Bhathiwal[3] ⓘ, Mozhgan Afshari[4]* ⓘ, G. B. Dharma Rao[5]* ⓘ

[1]*Department of Chemistry, Presidency University, Rajanukunte, Itgalpura, Bangalore, Karnataka, India.*
[2]*Department of Chemistry, Faculty of Science, SGT University, Chandu-Budhera, Gurugram, Haryana, India.*
[3]*Intertek India, Udyog Vihar, Phase I, Dundahera Village, Gurugram, Haryana, India.*
[4]*Department of Chemistry, Shoushtar Branch, Islamic Azad University, Shoushtar, Iran.*
[5]*Department of Chemistry, Kommuri Pratap Reddy Institute of Technology, Hyderabad, India.*

*Corresponding authors: mozhgan.afshari@iau.ac.ir, gbdharmarao@gmail.com

Abstract:

Continued research on pyrazoline derivatives with excellent biological activities has encouraged us to design and synthesize 1,3,5-trisubstituted pyrazoline series introducing NiFe₂O₄.Cu(OH)₂ magnetic nanocomposite as a heterogeneous catalyst by the combination of highly substituted aryl aldehydes, substituted acetophenones, and acetyl hydrazine hydrate under ultrasound irradiation at 50 °C. The NiFe₂O₄.Cu(OH)₂ magnetic nanocomposite materials are characterized by X-ray diffraction and Transmission electron microscopy. The characterized title compounds were studied for theoretical DFT studies using Spartan-14 software and molecular docking studies with Autodock Vina and Discovery Studio software to examine their antifungal activity efficiency against CaCYP51 (PDB ID-5EQB).

1. Introduction

Pyrazoles are a group of organic compounds with a simple aromatic ring and a heterocyclic series that Ludwig Knorr named in 1885 by the reduction of 1,3-diphenyl-5-methylpyrazole with sodium and ethanol [1]. Pyrazolines, furthermore known as dihydropyrazoles, are non-aromatic five-membered cyclic compounds holding two nitrogen atoms with one double bond. On the other hand, Fischer and Knövenagel addressed the synthesis of 2-pyrazoline analogs by the reaction of α,β-unsaturated aldehydes or ketones with hydrazines [2]. Particularly in developing synthetic processes and research into the bioactive qualities of the generated materials, heterocyclic chemistry has expanded quite quickly. In heterocyclic chemistry, the molecules with pyrazoline structures represent an important category. In the area of pharmaceutical and synthetic chemistry, these molecules are scaffold target compounds. These substances were utilized in the creation of agricultural and pharmaceutical products [3]. Pyrazoline compounds have been extensively researched for both their physical and biological characteristics. They have been utilized biologically as anti-bacterial, anti-HIV, anti-inflammatory, anti-amoebic, anti-fungal, anti-tuberculosis (TB), anti-trypanosomal, anti-tumor and anti-

leishmanial activity, antidepressant, and antipyretic [4–10]. On the other hand, some of the 2-pyrazolines derivatives have exciting optical character and consequently were used in fluorescent, fluorescent dyes and scintillators, sensors, and labeling agents [11]. Novel pyrazoline compounds with sulfonamide moiety were created and were discovered to be anti-inflammatory and anticancer agents, as shown in Figure 1 [12]. Pyrazolines have been employed extensively as key pharmacophores or as an intermediary in the synthesis of bioactive chemicals, and they have played a significant role in drug development research [13]. Some pyrazolines that have received patent protection have been used to treat food issues, such as obesity or metabolic syndrome in diabetic patients, as well as Type II diabetes and other related conditions [14]. Various protocols have been described for the synthesis of 2-pyrazolines with substitution, but broad-spectrum of outstanding methodologies accessible for the synthesis of different 2-pyrazolines are: i) reaction between hydrazines with α,β-unsaturated aldehydes and ketones, ii) reaction between diazoalkanes with α,β-enones and carboxylic acid esters, iii) reaction between olefins and α,β-enones with nitrilimines. Nitrilimines, diazoalkanes, and hydrazines are mostly used as common reactants for the source of nitrogen atoms in 2-pyrazoline, and only hydrazines that offer two of the nitrogen atoms in the 2-pyrazoline cyclic compound.

As emphasized, ultrasound irradiation (USI) has been a systematically fashionable technique in promoting an extreme range of organic transformations in the last decades, and it presides over a smooth-running platform for the synthesis of medicinally essential heterocyclic compounds [15–17]. It is a comparatively new-fangled approach for the interface of reactants and ultrasound energy, which encourages chemical and physical transformations. The traditional heating organic transformations that exercise strongly acidic circumstances, hazard reagents, elevated temperatures, prolonged reaction time, and unacceptable yields have been enhanced by ultrasonic accelerated organic transformations, representing less energy consumption with minimum production of unwanted products. On the other hand, USI had a broad range of applications from research laboratories to large-scale industries. The principle involved in ultrasound irradiation is the molecules of the solution will form small gas bubbles being developed, oscillate underneath a strong USI, and collapse in solution while being pretentious by USI, which produces sufficient energy for mechanical and chemical transformations.

At present, nanotechnology is experienced as an emerging trend in research laboratories as well as in large-scale industries and has a broad scope of applications, such as medicine, electronics, textile industries, and environmental remediation, owing to their special stupendous characteristics [18]. Furthermore, a huge extent of responsiveness was drawn to the NPs recommendations of several degrees of freedom for amendment of their catalytic properties as heterogeneous catalysts and accomplished a remarkable accountability in organic transformations because of unsophisticated work-up process, environmentally responsive, reusability, cost efficiency, and simplicity in separation. Nevertheless, heterogeneous metal catalysts that have experienced magnetic characteristics have unexpected attention from academic and industrial researchers for the reason of straightforwardness of separation after the achievement of reaction through the external magnet [19]. By considering the advantages of nanotechnology, herein we wish to study the application of synthesized $NiFe_2O_4.Cu(OH)_2$ magnetic nanocomposite
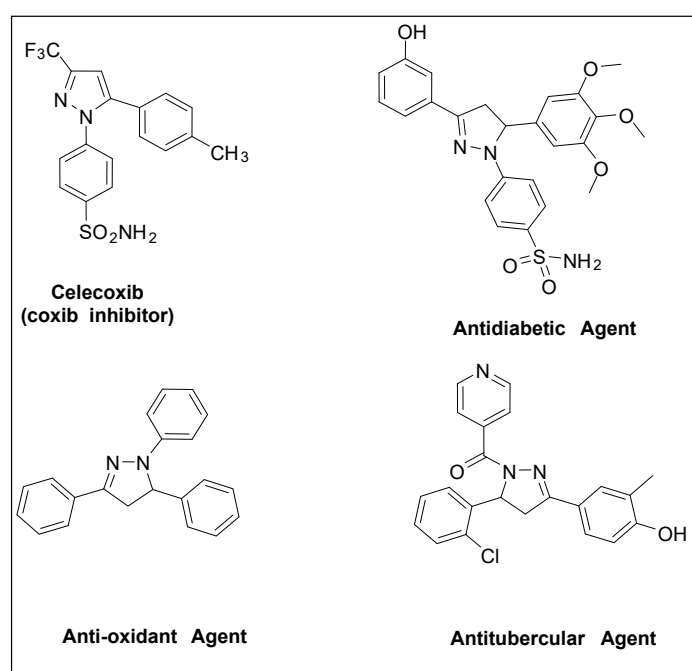
Figure 1. Pyrazoline core unit containing bioactive molecules.

[20] as a heterogeneous magnetic catalyst for the synthesis of 1,3,5-trisubstituted pyrazoline series derivatives.

Keeping in mind, from the support of literature standards and in continuation of our work in a laboratory for the synthesis of a library of bioactive molecules, there was a need to synthesize a series of pyrazoline derivatives because of sustainable chemistry and satisfactory yields in short reaction time [21–29]. By the above observance, herein we have paid more attention and addressed the synthesis of 1,3,5-trisubstituted pyrazoline derivatives by the reaction between highly substituted chalcone analogs with hydrazine hydrate using $NiFe_2O_4.Cu(OH)_2$ magnetic nanocomposite as heterogeneous catalyst under the irradiation of ultrasound as shown in Scheme 1. Besides this, we also acquire a chance to study the characteristics of the title compounds with density functional theory (DFT) and molecular docking.

2. Experimental

2.1 Synthesis of $NiFe_2O_4$ nanoparticle

Solutions of 0.5 M of $NiCl_2$ and 1.0 M of $FeCl_3$ were prepared separately in distilled water and thoroughly combined at 70 °C using a magnetic stirrer. After that, a burette was used to add 6.0 M NaOH solution dropwise until the pH of the solution reached 12. After stopping the addition of NaOH, the stirring was continued for another 1/2 hour. As a result of the reaction, a precipitate was generated. The resulting precipitate was agitated at 70 °C for 2.5 hours, then filtered and rinsed with ethanol and deionized water until pH 7 was achieved, and finally dried at 60 °C. To generate a crystalline product, the powder was calcined at 300 °C for 2.5 hours in a muffle furnace.

2.2 Synthesis of $NiFe_2O_4$/ Cu $(OH)_2$ nanocomposite

To create the $NiFe_2O_4/Cu(OH)_2$ nanocomposite, the generated $NoFe_2O_4$ nanoparticles (4.3m mol) are added to an aqueous solution of $CuCl_2$. $2H_2O$ (4.7 m mol). Behind that, add 1 M NaOH (6ml) solution slowly from the burette until the pH of the solution is attained to 13. Continue stirring for another 24 hours. The cooled precipitate was filtered and washed in distilled water before being dried at 60 °C [30].

2.3 General synthetic procedure for 1,3,5-trisubstituted pyrazoline derivative

In sequence to experiential the catalytic reactivity of $NiFe_2O_4.Cu(OH)_2$ magnetic composite, dried out 25 ml R.B flask fitted with a reflux condenser was packed with an arylaldehyde with substitution (1.0 mmol), acetophenone with substitution (1.0 mmol), and acetyl hydrazine hydrate (1.2 mmol) followed by the calculated amount of NaoH with 5.0 mol% $NiFe_2O_4.Cu(OH)_2$. The whole combined reactants were finely mixed and allowed for ultrasound irradiation for 30-50 min at 50 °C. The progress and end point of the reaction was examined on TCL. After the achievement of the reaction, the reaction temperature was decreased to room temperature, and the respective reaction mixture was cleaned with brine followed by the ethylacetate extraction. The $NiFe_2O_4.Cu(OH)_2$ magnetic composite was recovered using external magnetic retard and the organic solution was concentrated under reduced pressure followed by the wash with chilled diethylether to acquire the equivalent 1,3,5-trisubstituted pyrazoline derivative in a greater yield of 79-92%.

## 3. Results and Discussion

3.1 X-ray diffraction (XRD) analysis

Using Cu K radiation (=1.5418), a high-resolution X'Pert PAN analytical diffractometer with an Xe proportional detector was utilized to collect the PXRD pattern. It was recorded between 10 and 80 degrees at 25 °C with a scan rate of 4.0 seconds per step and a step size of 0.04◦. Measurements of Powder X-ray Diffraction (PXRD) were utilized to verify the cleanliness of the generated nanoparticles. The PXRD pattern reveals that the $NiFe_2O_4$ nanoparticles crystallize with tetrahedral and octahedral symmetry. The $NiFe_2O_4$ sample's crystallite size was discovered to be 39.44 and 45.24 nm using Debye-Scherrer analysis, as illustrated in Figure 2.

3.2 TEM analysis

FEI Technique G2 20 electron microscope was used to take TEM pictures of the $NiFe_2O_4.Cu(OH)_2$ nanocomposite at 200KV. The obtained $NiFe_2O_4.Cu(OH)_2$ nanocomposite's morphology was examined using TEM. The $NiFe_2O_4.Cu(OH)_2$ nanocomposite sample revealed a fully agglomerated spherical morphology, with crystalline size 42nm during TEM imaging as shown in Figure 3.

3.3 Vibration sample magnetometer (VSM)

The magnetic measurement was also carried out using a vibrating sample magnetometer (MPMS Excel Quantum Design USA) at room temperature. Fig. 4 shows the hysteresis loop of the composite sample. Broadening in the
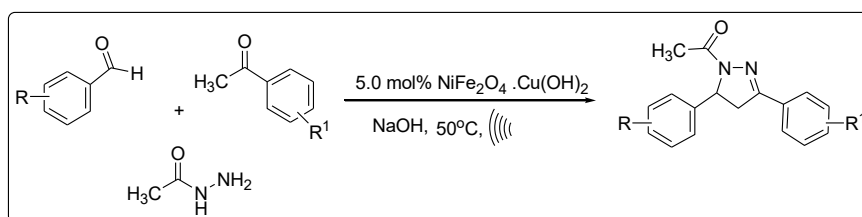
Scheme 1. Synthesis of pyrazoline derivatives using $NiFe_2O_4.Cu(OH)_2$ magnetic nanocomposite under ultrasound irradiation.
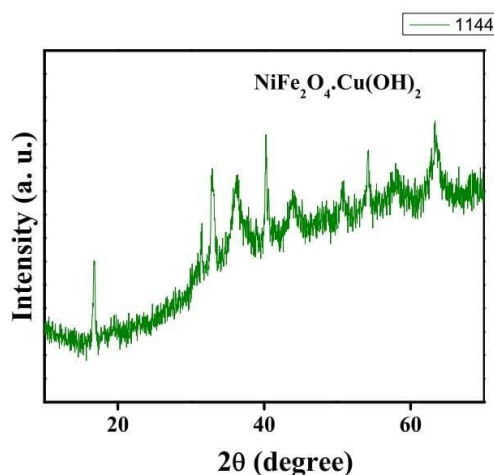
Figure 2. XRD analysis of $NiFe_2O_4.Cu(OH)_2$.

hysteresis loop indicates the nanoparticles' strong ferromagnetic behavior, which arises due to the coating of $Cu(OH)_2$ nanoparticles with $NiFe_2O_4$ nanospheres [31]. As per the measurement, it has been observed that $NiFe_2O_4/Cu(OH)_2$ nanocomposite shows a lower magnetization saturation (40 emu g^{-1}) than the uncoated nano nickel ferrite (128 emu g^{-1}), which may be due to the effect of $Cu(OH)_2$ shell coating and decreases the magnetostatic coupling between the particles.

3.4 Optimization of reaction conditions

To investigate the application of $NiFe_2O_4.Cu(OH)_2$ nanocomposite in the intended synthetic protocol, a reference reaction carried out by using benzaldehyde, acetophenone, and acetyl hydrazine hydrate at 50 °C, by varying the mole concentration of reactants using $NiFe_2O_4.Cu(OH)_2$ nanocomposite as heterogeneous catalyst under the irradiation of ultrasound. It was observed that, while benzaldehyde, acetophenone, and acetyl hydrazine hydrate were engaged in the 1:1:1.2 mole ratio using a $NiFe_2O_4.Cu(OH)_2$ magnetic nanocomposite underneath the irradiation ultrasound, ensuing in consequent 1-(3,5-diphenyl-4,5-dihydro-1H-pyrazol-1-yl)ethan-1-one and established as finest result in sight of reaction time and outstanding yield (**Table 2, Entry 1**).

The solvent in the reaction also played a significant role in achieving the target product. So, we planned to study solvent effect reference reaction (**Table 2, Entry 1**). First, we studied the reaction under solvent-free conditions, and we observed a 0% yield of the desired product. Furthermore, we studied the reaction with EtOH, H_2O, THF, CCl_4, and we found desired product yields as 92%, 79%, 32%, and 27%, respectively. From the above observations, it was found EtOH is a suitable solvent for the synthesis of the target compound under established conditions.

As of the above accessible reaction considerations, we examine the different mole concentrations of catalyst for the construction of pyrazoline derivative using heterogeneous $NiFe_2O_4.Cu(OH)_2$ nanocomposite catalyst at 50 °C by means of reference reaction (**Table 2, Entry 1**) and place the reaction time to 30 min as constant under irradiation of ultrasound. Performed the reference reaction under catalyst-free conditions using a mole ratio of 1:1:1.2 and observed the 42% yield of the corresponding pyrazoline and we also observed an increase in the yield of pyrazoline while increasing the mole concentration of catalyst. Nevertheless, among the entire catalytic concentrations, it was experiential that, 5.0 mol% of $NiFe_2O_4.Cu(OH)_2$ magnetic nanocomposite was determined to be the most important to attain the respective pyrazoline at 92% (**Table 2, Entry 1**). In contrast, it was also experienced that an increase in the mole concentration of the catalyst did not enhance the %
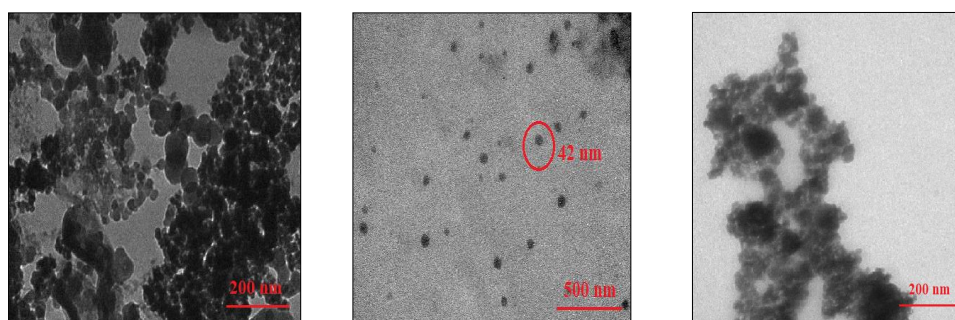

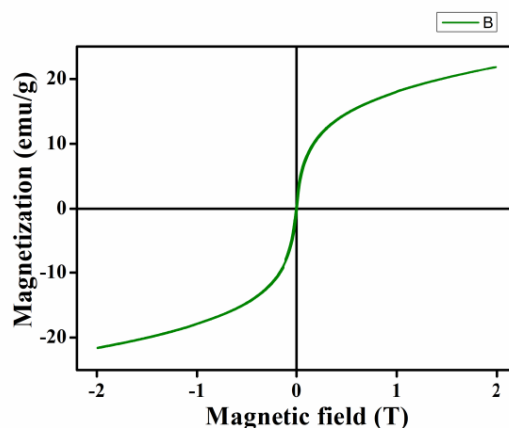**Figure 3.** TEM image of $NiFe_2O_4.Cu(OH)_2$ nanocomposite.

Figure 4. Magnetization curves $NiFe_2O_4.Cu(OH)_2$ nanocomposite.

yield of pyrazoline.

During exploratory reactions, we also studied the reference reaction (**Table 2, Entry 1**) in the same mole ratio of 1:1:1.2 underneath irradiation ultrasound for 30 min as set reaction duration by means of diverse nano catalysts enclosing with magnetic characteristics. Moreover, it was stated that the $NiFe_2O_4.Cu(OH)_2$ magnetic nanocomposite illustrates the most excellent outcome than distinguished with other magnetic nanocatalysts and the results are tabulated in Table 1. The practicability of these consistent reaction situations and substrate coverage of this reaction environment have furthermore lengthened to a broad range of arylaldehydes bearing an assortment of functional groups in addition to the assortment of acetophenone with different substitutions to synthesize the multi-functionalized pyrazoline derivatives. This methodology demonstrates the potential of both EWD and ED groups on arylaldehyde as well as on acetophenone recommend the respective 1,3,5-trisubstituted pyrazoline attained in good to satisfactory yields (79-92%), and entire final results were addressed in Table 2. The described procedure for the synthesis of 1,3,5-trisubstituted pyrazoline derivatives suggests supplementary rewards compared with those previously accounted in the literature, including reduced reaction duration, tolerated reaction circumstances, lack of chromatographic isolation, atom economy, and wide extent of substrate scope as contributed features. The novel $NiFe_2O_4.Cu(OH)_2$ catalyst could be effortlessly recollected by means of an outside magnetic and used again with no objectionable failure of catalytic activity.

### 3.5 Recyclability of $NiFe_2O_4.Cu(OH)_2$ magnetic composite material

As in the concern of the environment and sustainability view of assessment, capable of recovery and again the use of the catalyst is tremendously attractive. The catalyst as insoluble solid mass was recollected from the R.B container by means of external magnetic retard at the finishing point of the reaction from the reaction mixture and rinsed with warm ethanol, and activated at $350\,°C$ for 2.5 h to examine the reusability of $NiFe_2O_4.Cu(OH)_2$ magnetic composite material. The catalyst as solid mass was reprocessed in a similar process for 4 runs successive runs underneath the identical reaction situations and an alteration in catalyst experience was explored in terms of reaction duration and %yield. We inveterate that the equivalent 1,3,5-trisubstituted pyrazoline geometry (**Table 2, Entry 1**) accomplished acceptable % yields without substantial loss of any catalytic activity, as shown in Table 3.

Table 1. Effect of catalyst for the synthesis of 1,3,5-trisubstituted pyrazoline derivatives under irradiation of ultrasound.[a]

S.No	Name of the catalyst	Time (min)	(%) Yield [b]
1	$CaFe_2O_4$	30	82%
2	$CoFe_2O_4.Cu(OH)_2$	30	87%
3	$CuFe_2O_4$	30	83%
4	$NiFe_2O_4.Cu(OH)_2$	30	92%
5	$ZnFe_2O_4$	30	85%
6	Catalyst free	30	42%

a) Reaction conditions: Benzaldehyde (1.0 mmol), Acetophenone (1.0 mmol), Acetyl hydrazine hydrate (1.2 mmol) and various synthesized catalysts (5.0 mol %) under irradiation of ultrasound.
b) Isolated products

Table 2. NiFe$_2$O$_4$.Cu(OH)$_2$ magnetic composite catalyzed synthesis of 1,3,5-trisubstituted pyrazoline derivatives underneath irradiation of ultrasound circumstances.[a]
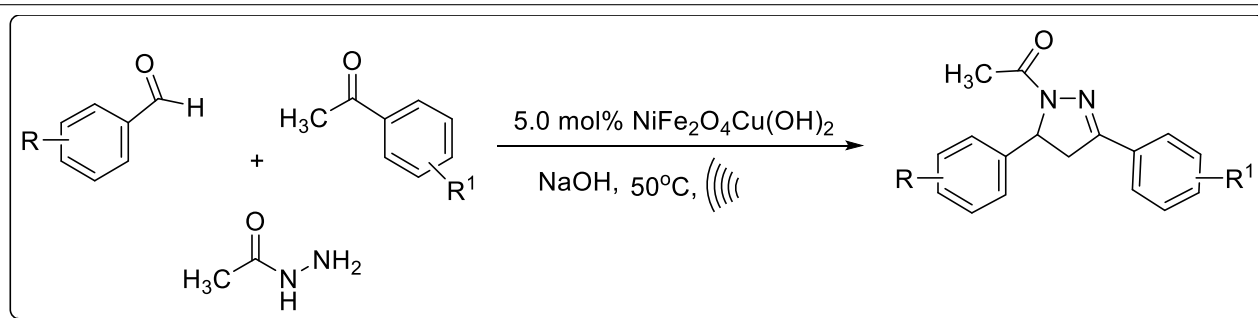
S.No.	R	R^1	Product[a]	Ultrasound irradiation Time (min)	Ultrasound irradiation %Yield[b]	Traditional Time (hr)	Traditional %Yield[b]	cLogP^c
1	4-H	4-H	**5a** (PYP-1)	30	92	6	89	3.157
2	4-NO$_2$	4-H	**5b** (PYP-2)	40	90	7	80	2.90
3	3-Cl	4-H	**5c** (PYP-3)	40	88	6	82	3.87
4	3-F	4-H	**5d** (PYP-4)	40	86	6	81	3.3
5	4-Cl	4-H	**5e** (PYP-5)	40	90	6	84	3.87
6	4-H	4-F	**5f** (PYP-6)	30	85	5	81	3.3
7	4-NO$_2$	4-F	**5g** (PYP-7)	45	91	7	80	3.043
8	3-Cl	4-F	**5h** (PYP-8)	45	86	7	78	4.013
9	3-F	4-F	**5i** (PYP-9)	45	88	7	75	3.443
10	4-Cl	4-F	**5j** (PYP-10)	45	82	7	75	4.013
11	4-H	3-Cl	**5k** (PYP-11)	30	91	5	78	3.87
12	4-NO$_2$	3-Cl	**5l** (PYP-12)	40	86	8	72	3.613
13	3-Cl	2-Cl	**5m** (PYP-13)	40	82	7	74	4.58
14	3-F	3-Cl	**5n** (PYP-14)	40	81	7	72	4.013
15	4-Cl	3-Cl	**5o** (PYP-15)	40	83	7	70	4.58
16	4-H	4-Cl	**5p** (PYP-16)	30	91	6	84	3.87
17	4-NO$_2$	4-Cl	**5q** (PYP-17)	40	83	8	74	3.613
18	3-Cl	2,4-Cl	**5r** (PYP-18)	50	81	8	72	5.29
19	3-F	2,4-Cl	**5s** (PYP-19)	50	79	8	70	4.73
20	4-Cl	2,4-Cl	**5t** (PYP-20)	45	85	8	76	5.29
21	4-H	4-OH	**5u** (PYP-21)	30	90	7	81	2.49
22	4-NO$_2$	4-OH	**5v** (PYP-22)	45	88	7	72	2.33
23	3-Cl	4-OH	**5w** (PYP-23)	40	90	8	77	3.203
24	3-F	4-OH	**5x** (PYP-24)	35	87	8	73	2.633
25	4-Cl	4-OH	**5y** (PYP-25)	40	85	8	71	3.203

[a]**Reaction conditions:** Substituted arylaldehyde (1.0 mmol), Substituted acetophonone (1.0 mmol) and acetyl hydrazine hydrate (1.2 mmol) at 50 °C using 5.0 mol% NiFe$_2$O$_4$.Cu(OH)$_2$ magnetic composite underneath irradiation of ultrasound.
[b]Isolated Yields
[c]cLog$P$ was estimated via chemdraw ultra 11.0v

Table 3. Reusability of the NiFe$_2$O$_4$.Cu(OH)$_2$ magnetic composite material for the synthesis of 1,3,5-trisubstituted pyrazoline (Table 1, Entry 1).

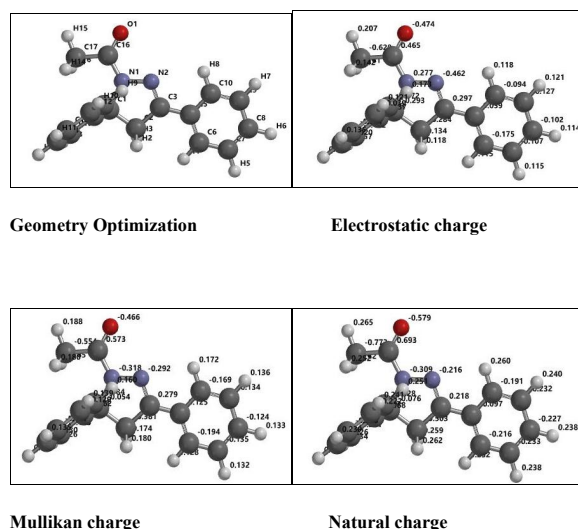| Cycles	1	2	3	4
% Yield	92%	89%	80%	71%

Figure 5. Molecular Geometry of compound PYP1.

3.6 Computational Studies

3.6.1 Molecular Geometry

Using the DFT/RB3LYP approach and the 6-31G (D) basis set, synthesized 1-(3,5-dihydro-1H-pyrazol-1-yl) ethan-1-one derivatives were accomplished at the DFT level. The following illustrates how the molecular geometry optimization of the generated compounds incorporates minimal energy of all substances tabulated in Table 4.

Figure 5 below illustrates the geometric optimization, electrostatic charges, Mullikan charges, and natural charges of compound **PYP 1**.

3.7 Frontier Molecular Orbital

Frontier molecular orbitals have been demonstrated to be significant for the optical, electric, and kinetic stability of chemical molecules in scientific studies and reports [32]. The values of the HOMO and LUMO orbitals are incredibly helpful in figuring out how molecules interact with one another. They are also thought to be useful in figuring out the compound's necessary molecular reactivity and stability. Additionally, the FMO of Pyrazoline compounds was calculated using the DFT/RB3LYP method and the

6-31G (D) basis set. A visual representation of HOMO and LUMO in the PYP 1 is shown in Figure 6.

3.8 Global Reactivity Descriptors

DFT was used to calculate the global reactivity characteristics of synthetic pyrazoline derivatives (density functional theory) [33]. Koopman's theorem was used to calculate the site selectivity and overall reactivity parameters of the synthesized pyrazoline derivatives. Janak's theorem [34] and Perdew et al. [35] calculations were used to determine the electron affinity and ionization potential of the synthesized pyrazoline derivatives are reported in Table 5.

3.9 Molecular electrostatic potential map

These maps give information on the behavior of chemical compounds and their reactivity with different molecules or species. Green, red, and blue patches on molecular potential maps, correspond to neutral, negative, and positive electrostatic potential regions, respectively [36]. The derivatives of the synthesized pyrazolines were used to create the MEP map, and the color range is shown in Figure 7.
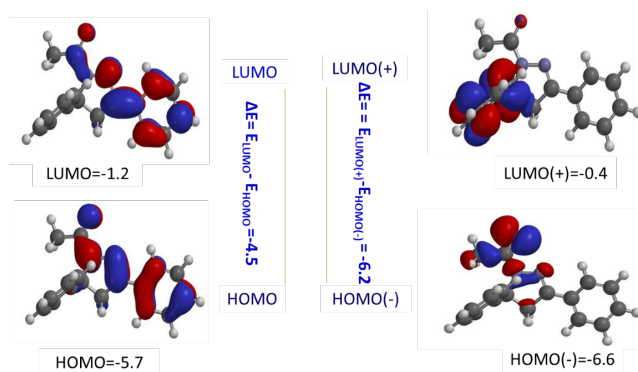

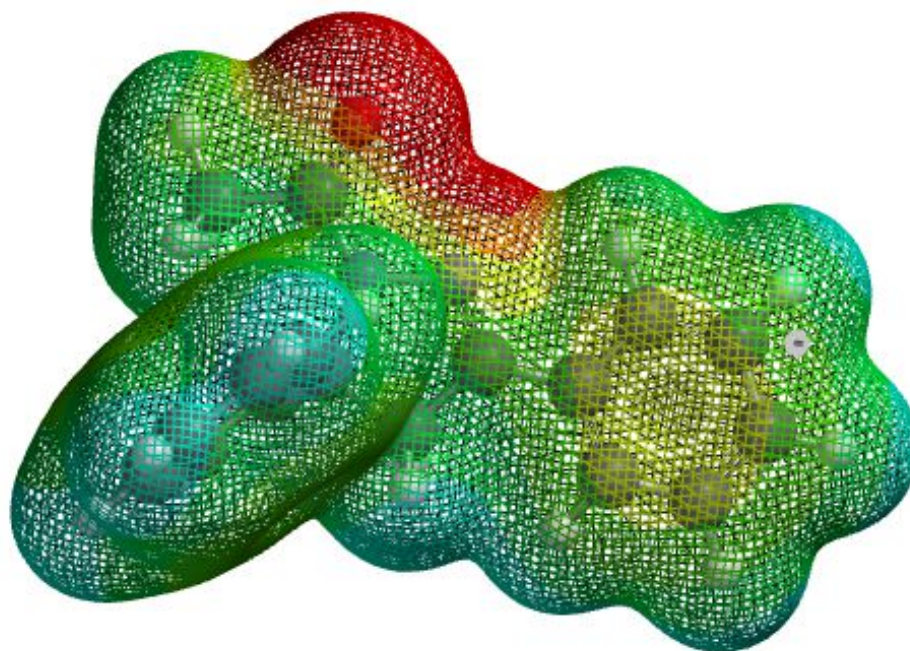**Figure 6.** Frontier Molecular Orbital of PYP 1.

Figure 7. MEP surface of PYP 1 compound.

Table 4. Energy, E_{HOMO}, E_{LUMO} Energy Gap, and Solvation Energy of Pyrazoline derivatives.

| S.No.	Code	Energy (au)	HOMO (eV)	LUMO (eV)	Energy Gap	Solvation (KJ/mol)
1	**PYP1**	-842.16	-5.7	-1.2	-4.5	-28.81
2	**PYP2**	-1046.66	-6	-2.6	-3.4	-34.69
3	**PYP3**	-1301.76	-5.8	-1.4	-4.4	-27.07
4	**PYP4**	-941.39	-5.8	-1.3	-4.5	-22.78
5	**PYP5**	-1301.76	-5.8	-1.4	-4.4	-29.31
6	**PYP6**	-941.39	-5.7	-1.3	-4.4	-23.27
7	**PYP7**	-1145.89	-6	-2.6	-3.4	-30.46
8	**PYP8**	-1400.99	-5.8	-1.4	-4.4	-22.01
9	**PYP9**	-1040.62	-5.8	-1.4	-4.4	-18.97
10	**PYP10**	-1400.99	-5.8	-1.4	-4.4	-24.26
11	**PYP11**	-1301.76	-5.9	-1.5	-4.4	-30.15
12	**PYP12**	-1506.25	-6.2	-2.7	-3.5	-36.27
13	**PYP13**	-1761.34	-6	-1.6	-4.4	-24.32
14	**PYP14**	-1400.99	-6	-1.6	-4.4	-24.43
15	**PYP15**	-1761.35	-6	-1.6	-4.4	-31.22
16	**PYP16**	-1761.34	-5.9	-1.7	-4.2	-22.38
17	**PYP17**	-1965.84	-6.2	-2.7	-3.5	-29.65
18	**PYP18**	-2220.94	-6.1	-1.8	-4.3	-21.95
19	**PYP19**	-1860.58	-6.0	-1.7	-4.3	-17.4
20	**PYP20**	-2220.94	-6.0	-1.8	-4.2	-22.64
21	**PYP21**	-917.38	-5.4	-1	-4.4	-49.64
22	**PYP22**	-1121.88	-5.7	-2.6	-3.1	-55.83
23	**PYP23**	-1376.97	-5.6	-1.2	-4.4	-48.12
24	**PYP24**	-1016.61	-5.5	-1.1	-4.4	-43.74
25	**PYP25**	-1376.97	-5.6	-1.2	-4.4	-50.27
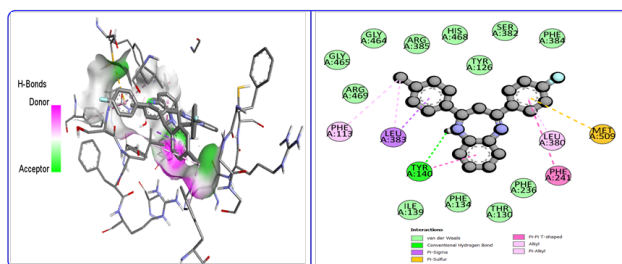
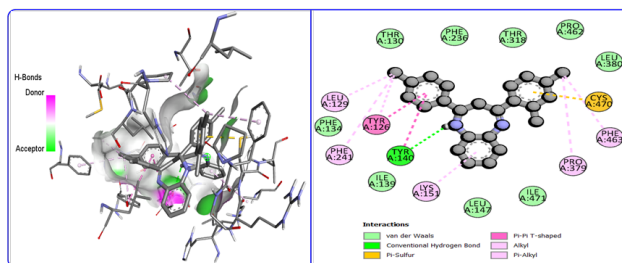Docking interaction of PYP 10 with CaCYP51 (PDB ID 5EQB).
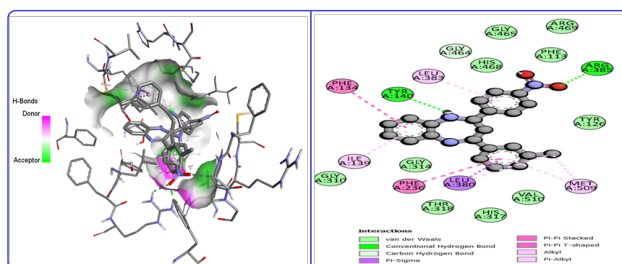
Docking interaction of PYP 12 with CaCYP51 (PDB ID 5EQB).
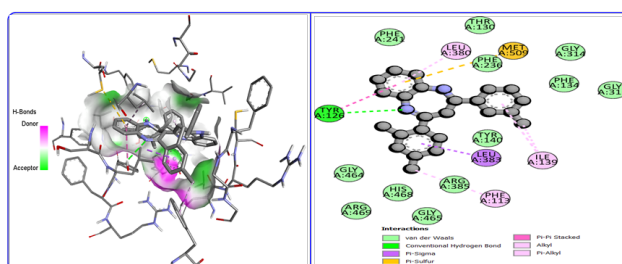
Docking interaction of PYP 18 with CaCYP51 (PDB ID 5EQB).
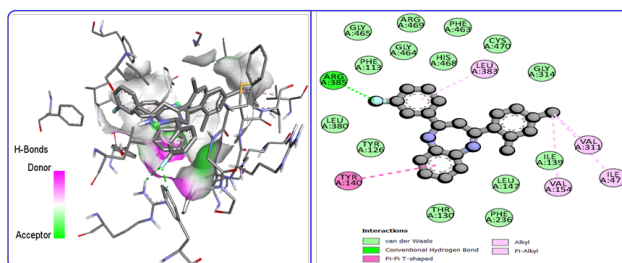
Docking interaction of PYP 19 with CaCYP51 (PDB ID 5EQB).

Docking interaction of PYP 20 with CaCYP51 (PDB ID 5EQB).

Figure 8. Docking interaction of compounds PYP 10, PYP 12, PYP 18, PYP 19, PYP 20 with CaCYP51 (PDB ID 5EQB).

Table 5. Global descriptors of twenty−five pyrazoline derivatives.

Code	IE	EA	X	μ	η	S	ω	ΔNmax	ΔE
PYP1	5.7000	1.2000	3.4500	-3.4500	2.2500	0.4444	2.6450	1.5333	-0.5625
PYP2	6.0000	2.6000	4.3000	-4.3000	1.7000	0.5882	5.4382	2.5294	-0.4250
PYP3	5.8000	1.4000	3.6000	-3.6000	2.2000	0.4545	2.9455	1.6364	-0.5500
PYP4	5.8000	1.3000	3.5500	-3.5500	2.2500	0.4444	2.8006	1.5778	-0.5625
PYP5	5.8000	1.4000	3.6000	-3.6000	2.2000	0.4545	2.9455	1.6364	-0.5500
PYP6	5.7000	1.3000	3.5000	-3.5000	2.2000	0.4545	2.7841	1.5909	-0.5500
PYP7	6.0000	2.6000	4.3000	-4.3000	1.7000	0.5882	5.4382	2.5294	-0.4250
PYP8	5.8000	1.4000	3.6000	-3.6000	2.2000	0.4545	2.9455	1.6364	-0.5500
PYP9	5.8000	1.4000	3.6000	-3.6000	2.2000	0.4545	2.9455	1.6364	-0.5500
PYP10	5.8000	1.4000	3.6000	-3.6000	2.2000	0.4545	2.9455	1.6364	-0.5500
PYP11	5.9000	1.5000	3.7000	-3.7000	2.2000	0.4545	3.1114	1.6818	-0.5500
PYP12	6.2000	2.7000	4.4500	-4.4500	1.7500	0.5714	5.6579	2.5429	-0.4375
PYP13	6.0000	1.6000	3.8000	-3.8000	2.2000	0.4545	3.2818	1.7273	-0.5500
PYP14	6.0000	1.6000	3.8000	-3.8000	2.2000	0.4545	3.2818	1.7273	-0.5500
PYP15	6.0000	1.6000	3.8000	-3.8000	2.2000	0.4545	3.2818	1.7273	-0.5500
PYP16	5.9000	1.7000	3.8000	-3.8000	2.1000	0.4762	3.4381	1.8095	-0.5250
PYP17	6.2000	2.7000	4.4500	-4.4500	1.7500	0.5714	5.6579	2.5429	-0.4375
PYP18	6.1000	1.8000	3.9500	-3.9500	2.1500	0.4651	3.6285	1.8372	-0.5375
PYP19	6.0000	1.7000	3.8500	-3.8500	2.1500	0.4651	3.4471	1.7907	-0.5375
PYP20	6.0000	1.8000	3.9000	-3.9000	2.1000	0.4762	3.6214	1.8571	-0.5250
PYP21	5.4000	1.0000	3.2000	-3.2000	2.2000	0.4545	2.3273	1.4545	-0.5500
PYP22	5.7000	2.6000	4.1500	-4.1500	1.5500	0.6452	5.5556	2.6774	-0.3875
PYP23	5.6000	1.2000	3.4000	-3.4000	2.2000	0.4545	2.6273	1.5455	-0.5500
PYP24	5.5000	1.1000	3.3000	-3.3000	2.2000	0.4545	2.4750	1.5000	-0.5500
PYP25	5.6000	1.2000	3.4000	-3.4000	2.2000	0.4545	2.6273	1.5455	-0.5500

It has been observed from Table 5, that **PYP12** and **PYP17** both show the highest value of **IE**, **EA**, **χ**, **µ**, **PYP1** and **PYP5** shows the highest value of **η**, **PYP2** and **PYP8** shows the highest value of **S**, **PYP12** and **PYP17** shows highest value of **ω**, **PYP22** shows highest value of **ΔNmax**, **PYP1**, **PYP4** shows highest value of **ΔE**.

3.10 Other molecular properties

The thermodynamic characteristics of chemical systems that can assist in understanding chemical processes were also calculated using density functional theory and quantum mechanics [37]. The details of the DFT calculation of the thermodynamic parameters at 1 atm pressure and 298.15K temperature using the B3LYP technique and 6-31G (D) basis set are provided in Table 6. For information on the charge density, reactivity index and charge distribution inside a molecule, the dipole moment and polarizability of the various molecular systems were also crucial chemical properties [38]. Table 3 contains the total number of synthesized Pyrazolines together with their determined thermodynamic properties, dipole moment, and polarizability.

3.11 Molecular docking studies

Utilizing the software program Discovery Studio Visualizer [39] and Auto dock Vina [40] molecular docking studies have been carried out to examine the interaction between pyrazoline derivatives and CaCYP51 (PDB ID 5EQB). the final compound PYP(1-25) had a specific binding affinity for the protein that causes fungal   infections in crops, as determined by molecular docking studies. **Table 7** lists the twenty-five molecules with the binding affinity (docking score).

The table reveals that the binding affinity of twenty-five compounds falls within the range of 9.4 to 10.8 kcal/mol. Figure 8 illustrates the identification of five compounds with the highest binding affinity for the CaCYP51 protein (PDB ID 5EQB), establishing a ligand-enzyme interaction. Among them, four compounds exhibit a binding affinity of 10.7 kcal/mol. notably; the compound PYP 18 engages in hydrogen bonding and achieves the highest binding score of 10.8 kcal/mol. According to the literature, it is acknowledged that compounds with a binding energy exceeding 7 kcal/mol can be regarded as potential candidates. In the context of pyrazoline derivatives, all the compounds exhibit a binding energy surpassing 9.4 kcal/mol. This suggests that these compounds can be deemed more promising than standard antifungal agents.
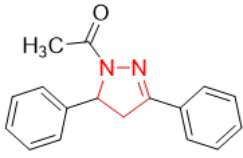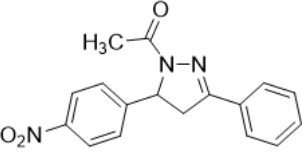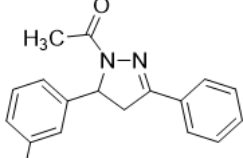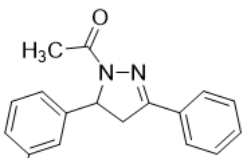
4. Conclusion

In outline, we have developed and established an unsophisticated and environmental compatibility procedure for the synthesis of 1,3,5-trisubstituted pyrazoline derivatives using NiFe$_2$O$_4$.Cu(OH)$_2$ magnetic nanocomposite as robust heterogeneous catalyst underneath irradiation of ultrasound. The significant qualities of this methodology
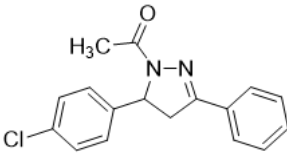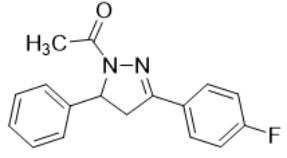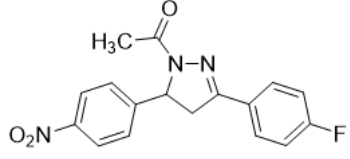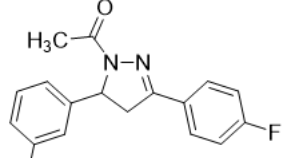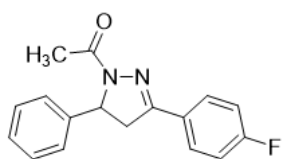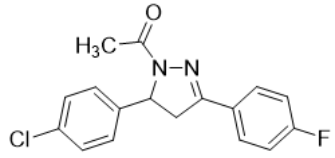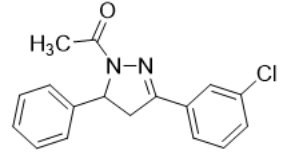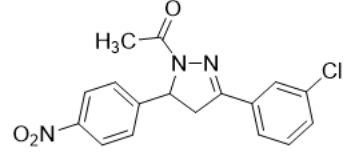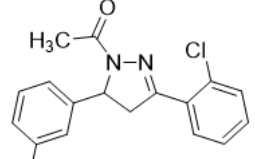
Table 6. Other Molecular properties of synthesized Pyrazoline compound.

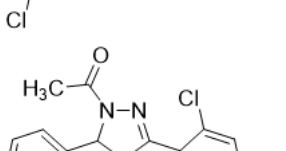| Code	Polarizability	Logp	D.M.(Debye)	ZPE(KJ/mol)	S^0	H^0	G^0	C_V	T_H	T_S
PYP1	63.58	2.00	5.29	771.42	487.05	-841.85	-841.91	209.75	186.782	136.071
PYP2	65.58	-0.43	5.67	778.03	522.89	-1046.35	-1046.41	232.22	188.363	150.376
PYP3	64.69	1.87	3.95	745.44	508.33	-1301.46	-1301.51	218.46	180.578	145.062
PYP4	63.95	1.47	4.23	749.51	500.81	-941.09	-941.15	217.12	181.544	141.357
PYP5	64.69	1.87	4.83	745.69	507.28	-1301.46	-1301.51	218.42	180.637	144.348
PYP6	63.96	1.47	5.55	749.63	500.4	-941.09	-941.15	217.36	181.573	140.216
PYP7	65.95	-0.97	5.39	756.2	535.93	-1145.59	-1145.65	239.87	183.144	154.549
PYP8	65.07	1.33	3.8	723.68	521.63	-1400.7	-1400.76	226.03	175.375	149.542
PYP9	64.29	0.93	4.44	728.76	513.48	-1040.33	-1040.39	223.25	176.585	141.057
PYP10	65.06	1.33	4.88	723.8	520.72	-1400.7	-1400.76	226.1	175.406	147.737
PYP11	64.71	1.87	7.03	745.39	508.27	-1301.46	-1301.51	218.44	180.565	144.535
PYP12	66.54	-0.57	6.49	753.88	543.36	-1505.95	-1506.01	239.72	182.596	140.611
PYP13	65.79	1.73	2.59	720.1	526.7	-1761.05	-1761.11	227.14	174.525	150.989
PYP14	65.09	1.33	5.68	723.37	521.81	-1400.7	-1400.76	225.9	175.301	149.694
PYP15	65.81	1.73	6.35	719.97	527.8	-1761.06	-1761.12	227.03	174.494	151.785
PYP16	65.82	1.73	4.64	719.87	527.27	-1761.05	-1761.11	227.13	174.47	145.174
PYP17	67.73	-0.71	4.23	726.91	562.34	-1965.55	-1965.61	249.58	176.154	163.695
PYP18	66.93	1.59	2.6	695.22	547.45	-2220.66	-2220.72	235.77	168.583	155.885
PYP19	66.19	1.19	3.16	698.65	540.83	-1860.29	-1860.35	234.59	169.397	154.521
PYP20	66.94	1.59	3.63	694.72	547.27	-2220.66	-2220.72	235.61	168.464	158.682
PYP21	64.17	0.92	4.03	781.94	504.67	-917.06	-917.12	222.1	189.296	141.136
PYP22	66.21	-1.52	5.09	788.52	540.28	-1121.56	-1121.62	244.6	190.871	155.569
PYP23	65.29	0.78	3.06	756.32	525.59	-1376.67	-1376.73	230.77	183.179	149.481
PYP24	64.55	0.38	3.18	760.45	518.24	-1016.3	-1016.36	229.4	184.16	145.648
PYP25	65.28	0.78	3.74	756.22	524.79	-1376.67	-1376.73	230.84	183.153	148.547
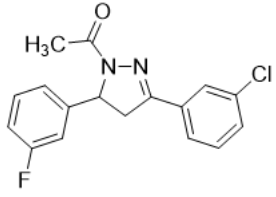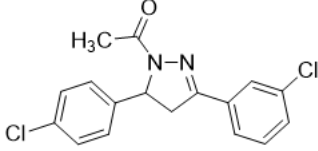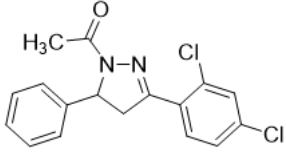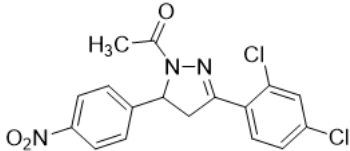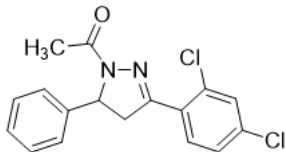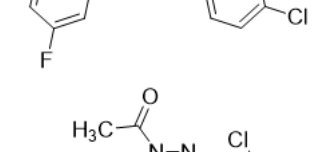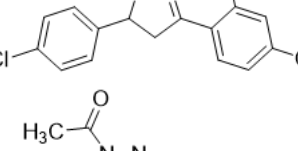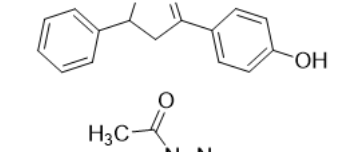
Table 7. Results of Molecular Docking Studies.

Ligands	Ligand Structure	Binding Affinity
PYP1		-10.0
PYP2		-10.4
PYP3		-10.1
PYP4		-10.0
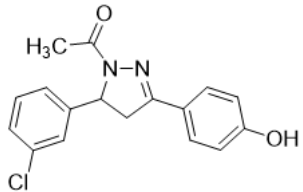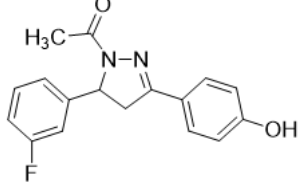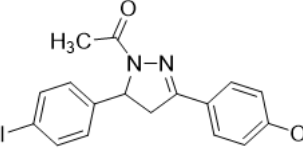
Continue of Table 7.

Ligands	Ligand Structure	Binding Affinity
PYP5		-10.4
PYP6		-9.9
PYP7		-10.2
PYP8		-10.3
PYP9		-10.2
PYP10		**-10.7**
PYP11		-9.9
PYP12		**-10.7**
PYP13		-10.2

Continue of Table 7.

Ligands	Ligand Structure	Binding Affinity
PYP14		-10.6
PYP15		-10.6
PYP16		-10.5
PYP17		-10.5
PYP18		**-10.8**
PYP19		**-10.7**
PYP20		**-10.7**
PYP21		-9.7
PYP22		-10.2

Continue of Table 7.

Ligands	Ligand Structure	Binding Affinity
PYP23		-10.1
PYP24		-9.8
PYP25		-9.4

are the effortless operation, tolerant reaction circumstances, straightforwardness of work-up, and extraordinary reusability of the magnetic nanocomposite catalyst. $NiFe_2O_4.Cu(OH)_2$ magnetic nanocomposite makes the reaction economical and the procedure an attractive alternative to the previously addressed literature for the formation of 1,3,5-trisubstituted pyrazoline derivatives. We believe the intention of the accessible procedure provided the preferred title compound in great to outstanding yields at reduced reaction duration, which might be owing to the superior reactivity of the reactants on the high surface area of $NiFe_2O_4.Cu(OH)_2$ magnetic nanocomposite. All compounds underwent initial DFT studies to determine their molecular geometry. The optimized structures were subsequently employed in molecular docking studies with the CaCYP51 protein (PDB ID 5EQB), utilizing Autodock Vina and Discovery Studio software. The assessment revealed that the binding affinities of these 25 compounds fall within the range of 9.4 to 10.8 kcal/mol, underscoring their potential as effective antifungal agents. The findings presented in this study provide a pathway for young researchers to explore the chemistry of pyrazoline analogs as potential antifungal drugs.

Authors Contributions
Authors have equal contribution role in preparing the paper.

Availability of Data and Materials
The data that support the findings of this study are available from the corresponding author upon reasonable request.

Conflict of Interests
The authors declare that they have no known competing financial interests or personal relationships that could have appeared to influence the work reported in this paper.

References

[1] R. H. Wiley, L. C. Behr, R. Fusco, and C. H. Jarboe. "chemistry of heterocyclic compounds.". (1967):177.

[2] A. Lévai. "". *Chem. Heterocycl. Compd.*, **33** (1997): 647–659. DOI: https://doi.org/10.1007/BF02291794.

[3] F. Turkan, A. Cetin, P. Taslimi, H. S. Karaman, and I. Gulcin. *Arch. Pharm.*, **352** (2019):1800359. DOI: https://doi.org/10.1002/ardp.201800359.

[4] S. Gomha, M. Abdalla, M. A. El-Aziz, and N. Serag. *Turk. J. Chem.*, **40** (2016):484–98, . DOI: https://doi.org/10.3906/kim-1510-25.

[5] M. M. Edrees, S. A. Melha, A. M. Saad, N. A. Kheder, S. M. Gomha, and Z. A. Muhammad. *Molecules*, **23** (2018):2970. DOI: https://doi.org/10.3390/molecules23112970.

[6] S. Abu-Melha, M. M. Edrees, S. M. Riyadh, M. R. Abdelaziz, A. A. Elfiky, and S. M. Gomha. *Molecules*, **25** (2020):4565. DOI: https://doi.org/10.3390/molecules25194565.

[7] A. R. Sayed, S. M. Gomha, F. M. Abdelrazek, M. S. Farghaly, S. A. Hassan, and P. Metz. *BMC chemistry*, **13** (2019):1–3. DOI: https://doi.org/10.1186/s13065-019-0632-5.

[8] S. M. Gomha, H. M. Abdel-aziz, M. G. Badrey, and M. M. Abdulla. *J. Heterocycl. Chem.*, **56** (2019):1275–82, . DOI: https://doi.org/10.1002/jhet.3487.

[9] A. O. Abdelhamid, S. M. Gomha, and W. A. El-Enany. *J. Heterocycl. Chem.*, **56** (2019):2487–93. DOI: https://doi.org/10.1002/jhet.3638.

[10] S. M. Gomha, M. A. Abdallah, I. M. Abbas, and M. S. Kazem. *Med. Chem.*, **14** (2018):344–55, . DOI: https://doi.org/10.2174/1573406413666171020114105.

[11] E. Bozkurt and H. I. Gul. *Sens. Actuators, B*, **255** (2018):814–825. DOI: https://doi.org/10.1016/j.snb.2017.08.062.

[12] M.N. Arshad, A.S. Birinji, M. Khalid, A.M. Asiri, K.A. Al-Amry, F.M. Aqlan, and A.A. Braga. *Spectrochim Acta A Mol Biomol Spectrosc.*, **202** (2018):146–158. DOI: https://doi.org/10.1016/j.saa.2018.04.069.

[13] A. Ahmad, A. Husain, S.A. Khan, M. Mujeeb, and A. Bhandari. *J. Saudi Chem. Soci.*, **20** (2016):577–584. DOI: https://doi.org/10.1016/j.jscs.2014.12.004.

[14] J. Jasril, I. Ikhtiarudin, S. Hasti, A.I. Indah, and N. Frimayanti. *Thai J. Pharm. Sci.*, **43** (2019):83–89.

[15] S. Saranya, S. Radhika, C. M. A. Abdulla, and G. Anilkumar. *J. Heterocycl. Chem.*, **58** (2021):1570–1580. DOI: https://doi.org/10.1002/jhet.4261.

[16] M. Draye, G. Chatel, and R. Duwald. *Pharmaceuticals*, **13** (2020):23. DOI: https://doi.org/10.3390/ph13020023.

[17] R. Chandan, S. Mehta, and R. Banerjee. *ACS Biomater. Sci. Eng.*, **6** (2020):4731–4747. DOI: https://doi.org/10.1021/acsbiomaterials.9b01979.

[18] H. Singh and K. Kaur. *Mater. Today Proc.*, (2023). DOI: https://doi.org/10.1016/j.matpr.2023.02.061.

[19] N. Zarei, M. Torabi, M. Yarie, and M. A. Zolfigol. *Polycycl. Aromat. Compd.*, **43** (2023):3072–3088. DOI: https://doi.org/10406638.2022.2061531.

[20] Z. M. Abbas, W. A. Shatti, M. M. Kareem, and Z. T. Khodair. *Chemical Data Collections*, **47** (2023):101078. DOI: https://doi.org/10.1016/j.cdc.2023.101078.

[21] S. A. C. Carabineiro, G. B. Dharma Rao, L. Singh, B. Anjaneyulu, and M. Afshari. *Processes*, **11** (2023):2294–2311. DOI: https://doi.org/10.3390/pr11082294.

[22] B. Anjaneyulu and G. B. Dharma Rao. *Lett. Org. Chem.*, **20** (2023):568–578. DOI: https://doi.org/10.2174/1570178620666230111103902.

[23] U. Jehangir, S. Khan, R. Hussain, Y. Khan, F. Ali, A. Sardar, S. Aslam, and M. Afshari. *Journal of Chemistry*, (2024):8426930. DOI: https://doi.org/10.1155/2024/8426930.

[24] R. Veligeti, J. S. Anireddy, R. B. Madhu, A. Bendi, P. L. Praveen, and D.S Ramakrishna. *J. Inorg. Organomet. Polym. Mater. 33.*, **12** (2023):4039–4051. DOI: https://doi.org/10.1007/s10904-023-02638-4.

[25] G. B. Dharma Rao, B. Anjaneyulu, M. P. Kaushik, and M. R. Prasad. *ChemistrySelect, 6*, **40** (2021):11060–11075. DOI: https://doi.org/10.1002/slct.202102949.

[26] M. Gorjizadeh and M. Afshari. *Russ. J. Gen. Chem., 87*, **4** (2017):842–845. DOI: https://doi.org/10.1134/S1070363217040284.

[27] S. Bhardwaj, B. Anjaneyulu, and L. Singh. *Curr. Org. Synth.*, **19** (2022):643–663. DOI: https://doi.org/10.2174/1570179419666220127143141.

[28] B. Anjaneyulu, S. Arti, G. B. Dharma Rao, M. J. Raza, and N. Sharma. *J. Chem.*, (2021):1–12. DOI: https://doi.org/10.1155/2021/7375058.

[29] G. B. Dharma Rao. *J. Heterocyc. Chem.*, **55** (2018): 2556–2562. DOI: https://doi.org/10.1002/jhet.3309.

[30] I. M. Khan, K. Alam, and M. J. Alam. *J. Mol. Liq.*, **310** (2020):113213. DOI: https://doi.org/10.1016/j.molliq.2020.113213.

[31] R. Eisavi and A. Karimi. *RSC Advances*, **9** (2019):29873–29887. DOI: https://doi.org/10.1039/C9RA06038C.

[32] J. Yu, N. Q. Su, and W. Yang. *J. Am. Chem. Soc.*, **6** (2022):1383–1394. DOI: https://doi.org/10.1021/jacsau.2c00085.

[33] T. V. Mourik, M. Buhl, and M.P. Gaigeot. "philos. trans.". *Math. Phys. Eng. Sci.*, **372** (2014):20120488. DOI: https://doi.org/10.1098/rsta.2012.0488.

[34] A. Gonis. *World J. Condens. Matter Phys.*, **4** (2014):78–83. DOI: https://doi.org/10.4236/wjcmp.2014.42012.

[35] J. P. Perdew, R. G. Parr, M. Levy, and J. L. Balduz Jr. *Phys. Rev. Lett.*, **49** (1982):1691–1694. DOI: https://doi.org/10.1103/PhysRevLett.49.1691.

[36] P. C. Agu, C. A. Afiukwa, O. U. Orji, E. M. Ezeh, I. H. Ofoke, C. O. Ogbu, E. I. Ugwuja, and P. M. Aja. *Sci Rep.*, **13** (2023):182409. DOI: https://doi.org/10.1038/s41598-023-40160-2.

[37] X. Y. Meng, H. X. Zhang, M. Mezei, and M. Cui. *Curr. Comput. Aided Drug Des.*, **7** (2011):146–57. DOI: https://doi.org/10.2174/157340911795677602.

[38] N. Ramasubbu, V. Paloth, Y. Luo, G. D. Brayer, and M. Levine. *J. Acta Crystallogr. D.*, **52** (1996):435–446. DOI: https://doi.org/10.1107/S0907444995014119.

[39] M. M. Kesavulu, S. Ramasubramanian, and K. Suguna. *Biochem. Biophys. Res. Commun.*, **331** (2005):1510–1514. DOI: https://doi.org/10.1016/j.bbrc.2005.03.247.

[40] O. Trott and A. J. J. Olson. *Comput. Chem.*, **31** (2010): 455–461. DOI: https://doi.org/10.1002/jcc.21334.